Numerical study of vortex matter using the Bose model: First-order melting and entanglement

Henrik Nordborg[a,b] and Gianni Blatter[a]
[a] *Theoretische Physik, ETH-Hönggerberg, CH-8093 Zürich, Switzerland*
[b] *Materials Science Division, Argonne National Laboratory, Illinois 60469*
(February 1, 2008)

We present an extensive numerical study of vortex matter using the mapping to 2D bosons and Path-Integral Monte Carlo simulations. We find a *first-order* vortex lattice melting transition into an *entangled* vortex liquid. The jumps in entropy and density are consistent with experimental results on $YBa_2Cu_3O_{7-\delta}$. The liquid is denser than the lattice and has a correlation length $l_z \approx 1.7\varepsilon a_0$ in the direction parallel to the field. In the language of bosons we find a sharp quantum phase transition from a Wigner crystal to a superfluid, even in the case of logarithmic interaction. We also measure the excitation spectrum of the Bose system and find the roton minimum to be insensitive to the range of the interaction.

74.20.De, 74.60.Ec, 05.30.Jp

I. INTRODUCTION

The Abrikosov mean-field theory of the vortex system predicts a peculiar continuous freezing transition, involving two symmetries, at the upper critical field H_{c2}[1]. The gauge symmetry is broken in the direction parallel to the field by the appearance of a superconducting order parameter $\Psi(\mathbf{x})$. The presence of the vortex lattice, on the other hand, leads to a periodic modulation of the amplitude of the order parameter, breaking the translational invariance of the system. This behavior contradicts a general argument by Landau, stating that breaking of continuous translation symmetry should be associated with a first order transition[2]. In order to resolve the paradox, we have to go beyond mean-field theory and take thermal fluctuations into account: The fluctuations melt the vortex lattice in a first-order transition at temperatures below the mean-field transition in agreement with the Landau argument[3]. The size of the region where thermal fluctuations are important is determined by the Ginzburg criterion: In conventional superconductors this region is small and mean-field theory offers a good description of the relevant physics. In the high-T_c materials, on the other hand, thermal fluctuations drastically change the mean-field phase diagram. Understanding the effect of thermal fluctuations is therefore vital for the understanding of the vortex state in high-T_c superconductors.

There exist a number of fundamental questions associated with the melting of the vortex lattice. To begin with, the existence of two symmetries naturally leads to the question of whether these have to be broken simultaneously in one transition[4]. In terms of vortices, the gauge symmetry along the field is destroyed by the alignment of the vortices with the applied magnetic field, whereas the translational symmetry is broken by the ordering of the lines in the direction transverse to the field. A melting scenario involving a disentangled liquid, which has been the topic of an intense scientific discussion over the past years[5,6], would break these symmetries in two separate transitions. A further topic deals with the properties of the melted phase: Is the resulting *vortex liquid* thermodynamically identical to the normal state or do further phase transitions exist at higher temperatures.

Although the importance of thermal fluctuations in the vortex system was recognized early[7,8,3], most progress has been made only in recent years. One important reason for this is that it has now become possible to observe the vortex lattice melting transition experimentally: After the first indirect observations based on resistivity measurements[9,10], more recent experiments have observed the first-order transition directly by measuring a jump in the magnetization or the latent heat[11–14]. The very large latent heat which was measured in many experiments was puzzling at first, but the problem has now been resolved satisfactorily[15,16].

On the theoretical side, there still does not exist a reliable theory for the vortex lattice melting transition. Early work using the renormalization group[3] or density functional theory[17] have indicated a first-order transition. Elastic theory has been combined with the Lindemann criterion to produce a melting line in good agreement with experimental observations[18,19]. Even though the Lindemann criterion does not give explicit information on the character of the melting line, it can be argued that the fact that it works so well gives support for a first-order transition. The question regarding the possible existence of a disentangled liquid has been addressed by analyzing the energy and stability of entangled configurations both in the liquid and in the lattice[20], with the conclusion that no disentangled liquid should exist.

The absence of an analytical description of the vortex lattice melting transition has led to a large interest in numerical simulations. A popular approach is to use the frustrated XY-model[21–28] or the closely related Lattice London model[29–32]. Unfortunately, many of the simulations have suffered from highly non-trivial finite-size

effects and have indicated two transitions instead of one at low filling factors, whereas a first-order transition was seen at large filling factors[22]. The problems have been overcome recently[25], and a picture with a single first-order transition is emerging. An overview of these problems can be found in Ref. 26. Simulations based on the Lowest Landau Level (LLL) approximation have shown a first-order vortex lattice melting transition[33] and obtained entropy jumps in agreement with experiments[15].

In this work we adopt a different approach from those described above. It was suggested by Nelson that the vortex system is equivalent to a system of interacting bosons in two dimensions[34]. This idea allows for using standard many-body techniques in describing the vortex system and has become a popular approach for analytical work on vortices[35–37]. The mapping to bosons, which we shall refer to as the *Bose model* in the following, has not been widely used for numerical work, however. This is perhaps surprising, since there exist numerical algorithms for simulating interacting bosons exactly. The main advantage of the Bose model lies in its generality: By analyzing this model, which contains very few adjustable parameters, we are able to obtain results for vortices, bosons, and interacting elastic lines, such as polymers, in general. Our approach also allows us to answer two questions which cannot be considered with the methods above. The first is obvious: How well does the Bose model describe the real vortex lattice? This has not been studied before, as it is difficult to make any quantitative predictions for strongly interacting bosons analytically. The second question is of a more fundamental nature: It has been known for a while that the 2D Bose Coulomb Liquid does not have a Bose-Einstein condensate even at $T = 0$[38–40]. Consequently, it has been questioned whether this system necessarily has to be crystalline or superfluid in its ground state, or whether some other phase might exist[5]. Here we show that the system has a direct transition from a crystal to a superfluid, and that a superfluid without a Bose-Einstein condensate can indeed exist.

Some early results of this work have been published previously[41]. Here we expand on our previous work, adding new results for melting in a compressible system using an isobaric Monte Carlo method. These results allow us to use the Clausius-Clapeyron relation as an consistency check on the simulation, since the change in density and the change in entropy can be measured independently at the transition. New results for the energy of corresponding Bose system are presented, and we discuss all results both in the language of bosons and vortices, further emphasizing similarities and differences between the two systems. Finally, specific details on the simulation are provided.

The outline of the paper is as follows: In Sec. II we describe the model and discuss its applicability to the vortex problem and the approximations made. We then turn to a qualitative description of the bosonic phase-diagram in Sec. III, and relate it to the phase diagram for vortices. The algorithm and the simulations are discussed in Sec. IV. Numerical results for the 2D Bose system are given in Sec. V and the numerical results for the vortex lattice melting transition are presented in Sec. VI. In Sec. VII we look at some properties of the vortex liquid and our conclusions are summarized in Sec. VIII. Three appendices provide technical details on various aspects of the simulation.

II. DESCRIPTION OF THE MODEL

A. Boson-vortex mapping

We consider a system of N bosons in two dimensions interacting through the potential $V(r) = g^2 \mathrm{K}_0(r/\lambda)$, where g^2 is the energy scale of the interaction, $\mathrm{K}_0(x)$ is a modified Bessel function of the second kind, and λ measures the range of the interaction. In the Feynman path-integral picture[42], the system is described by interacting "elastic" world-lines with the *imaginary-time* action

$$\frac{S}{\hbar} = \frac{1}{\hbar}\int_0^{\hbar/T} d\tau \left\{ \sum_i \frac{m}{2}\left(\frac{d\mathbf{R}_i}{d\tau}\right)^2 + \sum_{i<j} g^2 \mathrm{K}_0\left(\frac{R_{ij}}{\lambda}\right)\right\}. \tag{1}$$

Here, the two-dimensional vectors $\mathbf{R}_i(\tau)$ represent the positions of the bosons as a function of the imaginary time τ and T is the temperature of the system. The boundary condition for bosons is $\mathbf{R}_i(0) = \mathbf{R}_j(\beta)$, i.e., every line ends either on itself or on some other line. The partition function is the average of all possible line configurations subject to this boundary condition and weighted by the action (1):

$$\mathcal{Z}(T, A, N) \equiv \mathrm{e}^{-F(T,A,N)/T} = \frac{1}{N!}\int \prod_{i=1}^{N} \mathcal{D}\mathbf{R}_i \, \mathrm{e}^{-S/\hbar}, \tag{2}$$

where $F(T, A, N)$ denotes the Helmholtz free energy and A is the area of the system (we are considering two dimensions). It is often useful to consider a system of bosons at fixed chemical potential μ rather than at fixed number of particles. Switching ensemble is easily done according to

$$\mathcal{Z}(T, A, \mu) \equiv \mathrm{e}^{-\Omega(T,A,\mu)/T} = \sum_{N=0}^{\infty} \mathcal{Z}(T, A, N)\mathrm{e}^{\mu N/T}, \tag{3}$$

in which case $\Omega(T, A, \mu)$ denotes the grand-canonical potential.

It was pointed out by Nelson, that the action in Eq. (1) can also be interpreted as the London free-energy for a system of interacting vortices in type-II superconductors[34,43]. The starting point is the London free-energy functional

$$\frac{\mathcal{F}}{T} = \frac{1}{T}\int_0^{L_z} dz \left\{ \sum_i \frac{\varepsilon_l}{2}\left(\frac{d\mathbf{R}_i}{dz}\right)^2 + \sum_{i<j} 2\varepsilon_0 \mathrm{K}_0\left(\frac{R_{ij}}{\lambda}\right)\right\}, \tag{4}$$

where Φ_0 is the flux quantum, $\varepsilon_0 = \Phi_0^2/(4\pi\lambda)^2$ is the vortex line energy, L_z is the thickness of the sample, and ε_l is the elasticity of a vortex line. The latter depends strongly on the anisotropy and we have the estimate $\varepsilon_l \approx \varepsilon^2\varepsilon_0 \ln(a_0/2\sqrt{\pi}\xi)$, where $\varepsilon^2 < 1$ is the anisotropy parameter, ξ is the coherence length and a_0 is the lattice spacing. A detailed discussion of the line energy is given in Sec. II B. We will refer to Eq. (4) as the Bose model for the vortex system in the following.

Comparing Eqs. (1) and (4), and requiring $\mathcal{F}/T = S/\hbar$, we obtain the following formal mapping between 2D bosons and vortices:

$$\begin{array}{ccc} \tau & \leftrightarrow & z \\ \hbar & \leftrightarrow & T \\ g^2/\hbar & \leftrightarrow & 2\varepsilon_0 \\ \hbar/T_B & \leftrightarrow & L_z \\ m & \leftrightarrow & \varepsilon_l \end{array} \tag{5}$$

The temperature of the Bose system is denoted by T_B, in order to distinguish it from the (physically different) temperature T of the vortex system. Some conclusions can immediately be drawn from this mapping: The temperature of the vortex system corresponds to the Planck constant of bosons, implying that *thermal fluctuations* of vortices are equivalent to *quantum fluctuations* of bosons. Quantum fluctuations are more relevant for bosons with small mass. Since the mass of the bosons corresponds to the elasticity of the vortices, it follows that thermal fluctuations are more important for vortices with small elasticity, i.e., for anisotropic materials. Finally, the vortex system in a bulk superconductor, with $L_z \to \infty$, corresponds to the ground state, $T_B = 0$, of the bosons.

As in the case with bosons, it is often useful to consider a system where the number of vortices is allowed to fluctuate. The number of vortices determines the magnetic field and we therefore have to consider the Gibbs energy

$$\mathcal{G} = \mathcal{F} - \int d^3r \, \frac{HB}{4\pi}. \tag{6}$$

This quantity should be compared with $S/\hbar - N\mu/T_B$ for the bosons, and we obtain the formal equivalence

$$\frac{\mu}{\hbar} \leftrightarrow \left(\frac{\Phi_0 H}{4\pi} - \varepsilon_0 \ln\kappa\right). \tag{7}$$

The chemical potential μ is negative for $H < H_{c1} = \Phi_0 \ln\kappa/4\pi\lambda^2$, in agreement with the fact that no vortices enter the sample for fields below the lower critical field.

It will be convenient to introduce dimensionless parameters in the following analysis, which is done by choosing a length and an energy scale. As the length scale we take the lattice constant a_0 of a triangular lattice, i.e., the density is $\rho = 2/a_0^2\sqrt{3}$. The natural choice for the energy scale is g^2 for bosons and $\varepsilon_0 a_0$ for the vortex system. If we consider a fixed number of particles, where the chemical potential is not needed, the thermodynamic properties of the system are completely determined by the *three dimensionless parameters*

$$\Lambda \equiv \frac{\hbar}{a_0 g\sqrt{m}} = \frac{T}{a_0\sqrt{2\varepsilon_l\varepsilon_0}}, \tag{8a}$$

$$\beta \equiv \frac{g^2}{T_B} = \frac{2\varepsilon_0 L_z}{T}, \tag{8b}$$

$$\tilde{\lambda} \equiv \lambda/a_0, \tag{8c}$$

with the dimensionless action

$$S = \int_0^\beta d\tau \left\{ \sum_i \frac{1}{2\Lambda^2}\left(\frac{d\mathbf{R}_i}{d\tau}\right)^2 + \sum_{i<j} \mathrm{K}_0\left(R_{ij}/\tilde{\lambda}\right)\right\}. \tag{9}$$

The parameter Λ is the de Boer parameter and measures the size of fluctuations; *quantum* for bosons and *thermal* for vortices. This is the most important parameter in the present study. β is the dimensionless inverse temperature and we will only be considering the limit $\beta \to \infty$ here, corresponding to the ground state for bosons or vortices in a bulk superconductor. Finally, it is often a good approximation to use $\lambda = \infty$, which further reduces the number of parameters. In the latter case, we are studying the two-dimensional Bose Coulomb liquid (2DBCL) with logarithmic interaction. Note that simply taking the limit $\lambda \to \infty$ in the action (1) leads to a diverging energy and the interaction with a background charge therefore has to be subtracted. The density is then fixed by the requirement of charge neutrality and the system is therefore *incompressible*. In order to have a finite compressibility, which is needed for a density (or magnetization) jump at a first-order phase transition, we have to use a finite value of λ. Since the vortices in the XY-model interact logarithmically, it follows that this model will never have a magnetization jump, in contrast to recent claims[44].

B. Validity of the model

Before discussing the phase diagram of the model described above, we want to discuss its validity as a model for vortices in a type II superconductor. It is natural to divide this discussion into three parts, considering boundary conditions, linearization, and retarded interactions separately.

The Bose model differs from a real vortex system in the choice of boundary conditions: The natural boundary conditions for vortices are given by

$$\frac{d\mathbf{R}_i}{dz}(0) = \frac{d\mathbf{R}_i}{dz}(L_z) = 0, \tag{10}$$

since the screening currents, which encircle the vortex, cannot leave the sample. Since one cannot hope to simu-

late a sample with realistic dimensions we make use of periodic boundary conditions in all directions, as this minimizes the effect of the boundaries by ensuring $\nabla \cdot \mathbf{B} = 0$ everywhere. The expectation then is that the extrapolation of our numerical results to infinite system size provides an accurate description of the transition. The bosonic boundary conditions in the longitudinal direction, $\mathbf{R}_i(\beta) = \mathbf{R}_j(0)$, correspond to periodic boundary conditions for the magnetic field in the z-direction and have been used in most numerical simulations of vortices in bulk materials so far.

Another question is related to the linearization leading to the elastic term in Eq. (4), i.e.,

$$\frac{dl}{dz} = \sqrt{1 + \left(\frac{d\mathbf{R}}{dz}\right)^2} \approx 1 + \frac{1}{2}\left(\frac{d\mathbf{R}}{dz}\right)^2 \tag{11}$$

for an isotropic superconductor. This expansion is only valid as long as the vortex lines do not deviate too much from the z-axis. It is very accurate, however: For a vortex at a 30° angle with the z-axis, the error is roughly 1%. Close to the melting transition we have $(d\mathbf{R}/dz)^2 \approx c_L^2$, showing that the Taylor expansion is valid. Scaling theory proves this result to be true also in an anisotropic superconductor[45,35].

The use of the z-coordinate as a parameter for the vortex lines prohibits the formation of vortex loops in the ab-planes. Since these loops have been argued to be important for vortex lattice melting[31,27], we would like to remark on this point here. The free energy for a planar vortex loop of length L is given by

$$F_L = \left(\frac{L}{\xi}\right)\left[\varepsilon\varepsilon_0\xi - T\ln 3\right], \tag{12}$$

if we use a simple random walk argument for estimating the entropy. Loops will begin to proliferate when the free energy becomes negative, i.e., for $T > \varepsilon\varepsilon_0\xi/\ln 3$. This, however, is essentially the Ginzburg criterion, showing that planar vortex loops are important in the fluctuation regime close to the upper critical field H_{c2}. Due to the smallness of the Lindemann number for vortex lattice melting, the melting line is usually located well outside the fluctuation regime[4,19].

A more important approximation is the way the Bose model, i.e., Bosons with Yukawa interaction, neglects the "retarded" interaction of the real vortex lattice by the substitution[4]

$$\int dz' \frac{\mathrm{e}^{-\sqrt{R_{ij}(z,z')^2 + (z-z')^2}/\lambda}}{\sqrt{R_{ij}(z,z)^2 + (z-z')^2}} \Rightarrow \mathrm{K}_0\left[R_{ij}(z,z)/\lambda\right]. \tag{13}$$

We have used the notation $R_{ij}(z,z') = |\mathbf{R}_i(z) - \mathbf{R}_j(z')|$. Again, this approximation is valid as long as the lines are straight, at least over distances λ in the z-direction. However, Eq. (13) replaces a non-local interaction in the z-direction with a local one. The consequences of this can be understood in terms of the elastic properties of the vortex lattice: Since it is the non-local character of the interaction which produces dispersion, it follows that the substitution (13) will remove any k_z-dependence in the elastic moduli. The shear modulus c_{66} is not dispersive and remains unchanged. The compression modulus c_{11}, which is not important for vortex lattice melting, is changed in a trivial way. The tilt modulus, however, deserves a more detailed treatment. It is easy to see that the tilt modulus corresponding to Eq. (4) is given by

$$c_{44} = \frac{2}{\sqrt{3}}\frac{\varepsilon_l}{a_0^2}, \tag{14}$$

because only the self-energy terms contribute to the tilt energy. The real tilt modulus of the vortex lattice is rather complicated, especially in the case of layered materials[46,47,19]. The single vortex contribution is given by

$$c_{44}^0(K,k_z) \approx \frac{\varepsilon^2\varepsilon_0}{2a_0^2}\ln\left\{\frac{(\kappa/\varepsilon)^2}{1 + \lambda^2 K_{BZ}^2/\varepsilon^2 + \lambda^2 k_z^2}\right\} \tag{15}$$

and has the same form as Eq. (14) apart from a logarithmically weak k_z-dispersion. In addition, the real vortex system has a bulk contribution to the tilt, emanating from the interaction between vortices, which is given by

$$c_{44}(K,k_z) = \frac{B^2}{4\pi}\frac{1}{1 + \lambda^2 K^2/\varepsilon^2 + \lambda^2 k_z^2}. \tag{16}$$

This term is absent in the Bose model, since the interaction energy only depends on the distance between lines and not on their angle with the applied field. For thermal fluctuations, the relevant modes have wave vectors $K \approx K_{BZ} \approx \sqrt{4\pi}/a_0$ and $k_z \approx K/2\varepsilon$. Whence, the single-vortex part of the tilt modulus gives the dominant contribution to the stiffness of the lattice and we expect the Bose model to be valid for describing thermal fluctuations as long as we use Eqs. (14) and (15) to determine ε_l, i.e., by choosing $\varepsilon_l = \varepsilon^2\varepsilon_0\ln(a_0/2\sqrt{\pi}\xi)$.

The above discussion made use of the elastic moduli of the vortex lattice and is not directly applicable to the liquid. We do not know enough about the properties of the vortex liquid to be able to make an analytical comparison between the Bose model and the London model in this case. A major difference is that the vortex lines in the Bose model always repel each other, whereas the interaction between real vortices is proportional to the cosine of the angle between the lines and can become attractive. The difference is not important in the lattice, since the vortices are almost parallel anyway. In the liquid the vortices are not so well aligned and the difference will be larger. We argued above that the linearization of the self energy is very accurate, since the error is a fourth-order correction in dR_i/dz. Similarly, the error done by dropping the cosine is a second-order correction in the same quantity. The Bose model therefore still contains the main part of the interaction between the vortices and we

expect our results to be in rough quantitative agreement with those of the real system. This is further supported by the fact that our model correctly captures the properties of the vortex lattice melting transition, as will be shown below.

A very interesting consequence of the direction-dependent interaction for real vortices is the existence of an attractive van der Waals interaction even for straight vortices. This attractive interaction has important consequences for the low-field phase diagram of anisotropic superconductors, below the lower melting line[48]. For the magnetic inductions considered here, however, with $a_0 \lesssim \lambda$, the van der Waals interaction can safely be ignored.

III. THE PHASE DIAGRAM FOR BOSONS WITH LONG-RANGE INTERACTION

The phase diagram for Coulomb interacting bosons comprises three phases and is shown schematically in Fig. 1. The parameter Λ measures the size of quantum effects, and the line $\Lambda = 0$ therefore corresponds to the classical 2D Coulomb plasma. As the temperature is lowered, β is increased and we expect a transition from a fluid to a crystal. Numerical simulations agree on this transition being first order, taking place at $\beta_m \approx 140$[49–51]. For large quantum effects, i.e., for large Λ, the low temperature phase is a superfluid. The transition from a classical fluid to a superfluid is generally accepted to be a Kosterlitz-Thouless transition in two dimensions[52]. Finally, at large β, the system goes from a lattice to a superfluid as the size of quantum fluctuations is increased. Since no temperature is involved, this is a quantum phase transition, and the critical value of Λ is $\Lambda_m \approx 0.062$ for $\beta = \infty$[40]. This transition, which is equivalent to the vortex lattice melting transition in a superconductor, is the topic of the present study.

The phase diagram can be conveniently discussed in terms of three energy scales (potential, kinetic, and thermal) and two symmetries (gauge and translational). As long as the thermal energy $T_B = g^2/\beta$ dominates, the system possesses both global gauge invariance and continuous translational symmetry. If the potential energy g^2 dominates at low temperature, the translational symmetry is broken and we find a crystal. Otherwise, if the quantum mechanical kinetic energy $g^2\Lambda^2$ dominates, the gauge symmetry is broken and the system becomes superfluid. Strictly speaking, since we are in two dimensions, none of the symmetries is really broken at finite temperatures. Rather, both the crystal and the superfluid phase are characterized by *quasi long-range* order, as will be discussed below.

According to the phase diagram in Fig. 1 two symmetries must change simultaneously at the phase boundary between the crystal and the superfluid. This has led to speculations on the existence of other phases, such as the supersolid, in which both symmetries are broken. The first suggestion for the existence of such a supersolid phase in the context of superfluid He II was made by Andreev[53], see Ref. 54 for an overview. The topic has also been studied in the context of Josephson junction arrays, where a supersolid has been observed numerically[55], and for vortices in superconductors, where no supersolid was found[56].

Another suggestion is due to the rather peculiar properties of the 2D Bose Coulomb Liquid. It can be shown that the off-diagonal long-range order in the ground state decays as

$$\left\langle \psi^\dagger(\mathbf{r})\psi(0)\right\rangle \propto r^{-\alpha}, \tag{17}$$

where the exponent α is given by[5,40,39]

$$\alpha = \frac{1}{\Lambda}\left(\frac{\sqrt{3}}{16\pi}\right)^{1/2} = \left(\frac{mg^2}{8\pi\hbar^2\rho}\right)^{1/2} \approx \frac{0.186}{\Lambda}. \tag{18}$$

The system therefore does not have true off-diagonal long-range order (ODLRO) even in the ground state. This is in contrast to the case with short-range interactions where ODLRO decays algebraically only at finite temperatures according to the Hohenberg-Mermin-Wagner theorem[57]. The effect can be understood in terms of the long-range interaction suppressing long wavelength density fluctuations. Because of the uncertainty principle, this implies that the fluctuations in the conjugate variable, the phase, have to diverge.

The question is how large α can become before superfluidity is destroyed. One estimate is based on the analysis of the momentum distribution function: Computing the Fourier transform of Eq. (17) we obtain

$$n_{\mathbf{q}} \propto q^{\alpha-2}, \tag{19}$$

and the momentum distribution function actually vanishes for $q \to 0$ if $\alpha > 2$. Since the crystal melts at $\alpha_m \approx 3$ ($\Lambda_m \approx 0.062$), it is relevant to ask whether a 2D Bose liquid with $2 < \alpha < \alpha_m$ can be superfluid. Otherwise, a non-superfluid Bose liquid would exist at $T_B = 0$. One of the results of this work is to show that α can indeed be larger than 2 in a superfluid, and that superfluidity only disappears when the lattice forms, confirming the conjecture that a Bose system is either a superfluid or a crystal at $T_B = 0$. Note that the concept of a superfluid without a Bose-Einstein condensate is really not as striking as it might seem: A 2D Bose system does not have a real condensate at finite temperatures but can still be superfluid. Also, for He II in three dimensions, the condensate fraction is below 10% at zero temperature, whereas the superfluid density equals the total density[38].

A further consequence of the long-range interaction is that the solid phase appears at low densities, i. e., it is a Wigner crystal. For a finite interaction range λ, we also find a superfluid phase at low densities with $\lambda < a_0$. Finally, we note that since the interaction is purely

repulsive no generic liquid exists; the state which we refer to as a liquid might equally well be called a gas or a plasma.

It is instructive to discuss the phase diagram directly in terms of world lines. The partition function (2) includes all particle permutations, i.e., all ways of connecting the lower ends of the world lines at $\tau = 0$ with the upper ends at $\tau = \beta$, and most of the possible line configurations are heavily entangled. There are two factors that prevent this entanglement: The length of the world lines is determined by the temperature of the Bose system and the world lines can therefore only entangle if the temperature is low enough. A simple estimate for the entanglement temperature is given by

$$\frac{1}{\hbar}\frac{ma_0^2}{(\hbar/T_B)} = \frac{1}{\Lambda^2\beta} \approx 1, \tag{20}$$

marking the appearance of superfluidity. Since the interaction between the lines is also less effective at high temperatures, it follows that the high-temperature phase is a normal liquid. If the interaction is strong enough, it will prevent entanglement even of infinitely long world lines, and we have a crystal ground state.

The above phase diagram can be reinterpreted as a phase diagram for vortices by use of the parameter mapping in Eq. (8). The Wigner crystal corresponds to the vortex lattice, the superfluid is equivalent to an *entangled* vortex liquid, and the normal fluid corresponds to a *disentangled* vortex liquid. Since the parameter β is proportional to the thickness of the sample, we are only interested in the limit $\beta \to \infty$ for a bulk superconductor. It is important to use a large enough L_z in a numerical simulation: The dashed line in Fig. 1 shows the curve obtained by keeping B (a_0) constant and varying T for some finite L_z. The curve passes from a lattice, via a disentangled vortex liquid, into an entangled liquid. As L_z is increased, however, the curve is pushed to higher values of β and we have a direct transition from a lattice to an entangled liquid.

IV. NOTES ON THE ALGORITHM

One of the advantages of using the Bose model for describing the vortex system is that there exist well established algorithms for simulating bosons numerically exactly. The ground state of a Bose system can be studied using variational and diffusion Monte Carlo methods, which has been done for the system considered here by Ceperley and Magro[58,40]. They observed the disappearance of the Wigner lattice as Λ was increased and also studied the momentum distribution function in the liquid, which agreed with the result in Eqs. (17) and (18). Simulations at $T_B = 0$ are usually not very good at computing response functions, such as the superfluid density, since these depend on the excitations available in the system rather than on the ground state wavefunction. Although this difficulty can be overcome for the special case of the superfluid density[59], we have chosen the more conventional approach of simulating a system at finite temperature. Not only does this allow us to compute the superfluid density using the winding number, but it also allows us to study the excitation spectrum from the dynamic structure factor.

Exact finite temperature simulations on Bose systems were introduced by Ceperley and Pollock and applied to superfluid He II in two and three dimensions[60–62]. The method is known as the Path Integral Monte Carlo (PIMC) method, and differs from the more widely used world-line methods in that it does not introduce a lattice. It is therefore possible to obtain numerically exact results for realistic interactions between the bosons, as has been amply demonstrated by Ceperley and co-workers in computing the superfluid density and the excitation spectrum for superfluid He II[63].

The method involves discretizing the imaginary time in the path integral for the partition function, which, in the Trotter approximation, becomes

$$\mathcal{Z}(\beta,\Lambda,N) = \frac{1}{N!}\left(\frac{1}{2\pi\Lambda^2\tau}\right)^{MN}\int\prod_{m=1}^{M}\prod_{i=1}^{N} d^2R_{i,m}\mathrm{e}^{-S[\{\mathbf{R}_i]\}}, \tag{21}$$

with

$$S[\{\mathbf{R}_i\}] = \sum_{i,m}\frac{\left(\mathbf{R}_{i,m+1}-\mathbf{R}_{i,m}\right)^2}{2\Lambda^2\tau} + \sum_{i<j,m}\tau\mathrm{K}_0\left(R_{ij,m}/\lambda\right). \tag{22}$$

Here the indices (i,j) label the particles, m labels the Trotter slices ranging from 1 to M, and we have $\tau = \beta/M$ for the size of the imaginary time step. We have typically used $M = 100$ and $N = 25 - 100$ in the simulations presented here, with periodic boundary conditions in all directions. A rhombically shaped system, with the smaller angle equal to 60°, has been used to allow for a triangular lattice without frustration. Since the range of the interaction is usually larger than the size of the system, it is important to account for the periodicity of the system also in the interaction. We do this by solving the London equation with the correct boundary conditions and the resulting expressions are given in Appendix A.

Computation of thermodynamic averages using Eq. (21) involves evaluating a multi-dimensional integral numerically. Since the dimensionality is high, with $MN \approx 10^3 - 10^4$, an efficient algorithm is needed. Most of the PIMC algorithm, including the bisection method for generating new line configurations, is described in the review by Ceperley[63]. There is one point, though, where our algorithm differs from those used before: In order to capture the quantum effects correctly in the Bose system, it is necessary to sample the particle permutations accurately. Thus we have to probe all ways of connecting

the lower ends of the lines $\mathbf{R}_i(0)$ with the upper ends $\mathbf{R}_i(\beta)$. Usually this is done by allowing a small number of lines to change their endpoints in every Monte Carlo update. We were unable to equilibrate the system using any such algorithm. Rather we use a random walk algorithm which allows the system to choose a permutation of a large number of lines according to its statistical weight. The algorithm is described in Appendix B. For N = 49 or less, we actually do this random walk in the space of the permutations of all N lines, leading to a reasonably fast convergence of the winding number (see below).

A. Thermodynamic properties

We now turn to the measurable quantities of the system. The existence of a lattice is tested by measuring the structure factor $S(\mathbf{Q})$,

$$S(\mathbf{Q}) = \frac{1}{N}\langle\rho(\mathbf{Q})\rho(-\mathbf{Q})\rangle = \frac{1}{MN}\left\langle\sum_{ij,m}\exp\left\{i\mathbf{Q}\cdot(\mathbf{R}_{i,m}-\mathbf{R}_{j,m})\right\}\right\rangle, \quad (23)$$

where the same convention for the sums has been used as in Eq. (21) and we use $\langle\ldots\rangle$ to denote Monte Carlo averages. The height of the structure factor evaluated at a reciprocal lattice vector scales with the size of the system. More specifically, we have

$$S\left(\mathbf{Q}_1\right) = N\exp\left\{-\frac{8\pi^2}{3a_0^2}\langle u^2\rangle\right\} \quad (24)$$

for the first Bragg peak in the triangular lattice, where $\langle u^2\rangle$ denotes the mean-squared fluctuations. Expression (24) has the usual Debye-Waller form and requires the lines to fluctuate harmonically around their average positions.

We stated above that there should be no true long-range order in a system of finite thickness (β). Consequently, there should not exist real Bragg peaks. In order to understand this point better, we compute $\langle u^2\rangle$ using elastic theory for a system of finite thickness. The main contribution comes from transverse fluctuations, given by the expression

$$\frac{1}{2}\langle[u_\perp(\mathbf{R})-u_\perp(0)]^2\rangle = \frac{1}{L_z}\int\frac{d^2K}{(2\pi)^2}\sum_{k_z}\frac{T\left[1-\cos(\mathbf{K}\cdot\mathbf{R})\right]}{c_{66}K^2+c_{44}k_z^2}. \quad (25)$$

Here, the two-dimensional K integral is over the Brillouin zone, with $K_{BZ}=\sqrt{4\pi}/a_0$, and the discrete k_z-vectors are given by $k_z = 2\pi n/L_z$. We ignore the dispersion of the tilt modulus for the moment. Separating off the $k_z = 0$ term and integrating over the remaining ones, we obtain

$$\frac{1}{2}\langle u_\perp(\mathbf{R})-u_\perp(0)]^2\rangle \approx \frac{TK_{BZ}}{4\pi\sqrt{c_{66}c_{44}}}+\frac{T}{2\pi c_{66}L_z}\ln(R/a_0) \quad (26)$$

in the limit $R \gg a_0$. The first term is the result for the transverse fluctuations in a bulk superconductor and contains only $k_z \neq 0$ modes. The second term is due to the $k_z = 0$ mode and thus corresponds to motion of the average position of a vortex line. In a sample of finite thickness there is always only quasi long-range order since the second term in Eq. (26) grows logarithmically with the distance R. This term, however, is only relevant if $R \gtrsim a_0\exp\left(c_{66}a_0^2L_z/T\right)$, which grows exponentially with the thickness of the sample. In the limit $L_z \to \infty$, the second term of Eq. (26) vanishes and we recover the well known result of true long-range order in the Abrikosov lattice.

We shall use the bosonic superfluid density as a measure of the entanglement in the system. The superfluid density is defined by the response of the system to a transverse gauge field, or, equivalently, to the motion of the walls of the container. We therefore have to study a system described by the Hamiltonian $H_{\mathbf{v}}$, obtained from the original Hamiltonian by the transformation $\mathbf{p} \to \mathbf{p} - m\mathbf{v}$. The superfluid density is then given by

$$\frac{\rho_s}{\rho} = \frac{1}{mN}\frac{\partial^2}{\partial\mathbf{v}\partial\mathbf{v}}F_{\mathbf{v}}(\beta,\Lambda) = -\frac{T_B}{mN}\frac{\partial^2}{\partial\mathbf{v}\partial\mathbf{v}}\ln\mathcal{Z}_{\mathbf{v}}(\beta,\Lambda), \quad (27)$$

where $F_{\mathbf{v}}$ and $\mathcal{Z}_{\mathbf{v}}$ represent the free energy and the partition function for the system with moving walls. It can be shown that the latter is given by[63]

$$\mathcal{Z}_{\mathbf{v}}(\beta,\Lambda) = \mathcal{Z}_0(\beta,\Lambda)\exp\left\{\frac{im}{\hbar}\mathbf{W}\cdot\mathbf{v}\right\}, \quad (28)$$

where the winding vector $\mathbf{W}$ is defined as

$$\mathbf{W} = \sum_i\int d\tau\frac{d\mathbf{R}_i}{d\tau}. \quad (29)$$

This definition deserves an explanation. Since the upper ends ($\tau = \beta$) are just a permutation of the lower ends ($\tau = 0$), the only paths which give a contribution to the winding number are those which leave the system on one side and return on another via the periodic boundary conditions. For these paths we have

$$\int d\tau\frac{d\mathbf{R}_i}{d\tau} = \mathbf{R}_i(\beta)-\mathbf{R}_i(0)+L\mathbf{n}, \quad (30)$$

where L is the linear size of the system and $\mathbf{n} \in \mathbb{Z}^D$ is an integer vector. We are only considering $D = 2$ in this work, but the winding number definition of the superfluid

density is valid in any dimension D. Combining Eqs. (27) and (28) we immediately arrive at

$$\frac{\rho_s}{\rho} = \frac{\langle W^2 \rangle}{D\Lambda^2 \beta N}, \tag{31}$$

which is an exact relation. It turns out, however, that it is numerically difficult to get good statistics for the winding number in large systems since it can only be changed by global moves involving on the order of $\sqrt[D]{N}$ world lines. For large systems we then made use of a simpler measure of quantum effects, which consists of simply counting the number of world lines which do not end on themselves:

$$N_e \equiv \text{number of lines with } \mathbf{R}_i(\beta) \neq \mathbf{R}_i(0). \tag{32}$$

This quantity does not need any global moves to be changed and is therefore simple to measure for arbitrarily large systems. It is interesting to consider the relation between N_e and ρ_s. Obviously $N_e > 0$ is a necessary condition for $\rho_s > 0$. There is no guarantee, however, that the condition is also sufficient. In order to arrive at a more quantitative relation between the two quantities, we can reason as follows: The quantities ρ_s/ρ and N_e/N are intensive and should not depend on the total number of particles in the system. If we assume that they are proportional to each other, it follows from Eq. (31) that

$$\langle W^2 \rangle \propto N_e, \tag{33}$$

which is reasonable, given that the vector $\mathbf{W}$ is the sum of N_e randomly directed vectors. Unfortunately, we cannot offer a derivation of the proportionality constant in Eq. (33) and thus have to rely on empirical results: We define the quantity ρ_e according to

$$\frac{\rho_e}{\rho} \equiv \frac{\alpha(\Lambda,\beta)}{D\Lambda^2\beta}\frac{N_e}{N} \tag{34}$$

and compute $\alpha(\Lambda,\beta)$ by requiring $\rho_e = \rho_s$ for small systems where ρ_s can be computed using the standard winding number definition (31). It turns out that for the range of parameters considered here, we can ignore the Λ and β dependence of $\alpha(\Lambda,\beta)$ and use

$$\alpha(\Lambda,\beta) = 4.04. \tag{35}$$

We emphasize, however, that $\alpha(\Lambda,\beta)$ does depend on both β and Λ in general. Fig. 2 shows the superfluidity, measured according to Eqs. (31) and (34), as a function of Λ for two different system sizes. The good agreement between ρ_e and ρ_s, particularly the sharp onset of ρ_e at melting (see Fig. 4), is a consequence of the strong first-order character of the transition, and makes us confident that ρ_e provides a good estimate for the superfluid density in the larger Bose systems. Nonetheless, we stress that ρ_e is not a real order parameter since, in contrast to ρ_s, it does not vanish in the lattice phase when taking the thermodynamic limit.

The energy of the system, both for bosons and vortices, can be computed using the thermodynamic definition

$$E = T^2 \frac{\partial}{\partial T} \ln \mathcal{Z}(\Lambda,\beta). \tag{36}$$

Due to the different temperature dependence of the parameters Λ and β in the two cases, the resulting expressions for the energy are different. It is useful to define the two expectation values

$$S_1 = \left\langle \sum_m \sum_i \frac{(\mathbf{R}_{i,m+1} - \mathbf{R}_{i,m})^2}{2\Lambda^2\tau} \right\rangle \tag{37a}$$

$$S_2 = \left\langle \sum_m \sum_{i<j} \tau \mathrm{K}_0\left(R_{ij,m}\right)/\lambda \right\rangle \tag{37b}$$

corresponding to the two terms of the action (22). The important point is the temperature dependence of the term S_1. For bosons, we have $\tau \propto 1/T_B$ and $S_1 \propto T_B$. The expression for the energy then becomes[63]

$$E_B = T_B(MN - S_1) + T_B S_2, \tag{38}$$

where the two terms correspond to kinetic and potential energies, respectively. The quantum-mechanical kinetic energy is decreased by the fluctuations of the world lines, since the fluctuations correspond to a smearing of the wave function.

In the case of vortices, the denominator of S_1 is given by

$$\Lambda^2\tau \propto \frac{T}{\varepsilon_l}. \tag{39}$$

If we want to treat $\mathcal{F}$ as a model Hamiltonian, we should ignore its internal temperature dependence through the penetration depth $\lambda(T)$. In this case, ε_l and ε_0 are constants and both the terms S_1 and S_2 are proportional to $1/T$. Computing the temperature derivative in Eq. (36) we obtain

$$\langle \mathcal{F} \rangle = T(S_1 - MN) + TS_2, \tag{40}$$

where $\mathcal{F}$ is again the Ginzburg-Landau free energy functional. The expectation value of $\mathcal{F}$ is a very useful quantity to measure, but does not represent the energy of the vortex system. As was pointed out by Hu and MacDonald[15], the internal temperature dependence of $\mathcal{F}$, through $\lambda(T)$, accounts for microscopic degrees of freedom that give a significant contribution to the energy. We will show below how Eq. (40) can be combined with scaling properties of the London free energy to obtain the correct expression for the energy.

Another advantage of doing the simulation at finite temperature is that it allows us to compute the excitation spectrum of the system. The idea is to analyze the

dynamic structure factor $S(\mathbf{Q}, i\omega_n)$, which can be obtained as the partial Fourier transform of the retarded density correlator

$$S(\mathbf{Q}, \tau) = \frac{1}{N} \langle \rho(\mathbf{Q}, \tau) \rho(-\mathbf{Q}, 0) \rangle \,. \tag{41}$$

The normalization is chosen so that $S(\mathbf{Q}, \tau = 0)$ is the static structure factor of Eq. (23). The standard method for obtaining the excitation spectrum from $S(\mathbf{Q}, i\omega_n)$ is to perform an analytic continuation to real frequencies using the maximum entropy method (see Ref. 64 for an overview). Here we use a simpler approach, similar in spirit to analytical work by Nelson and Seung[43]. If we assume the structure factor at momentum $\mathbf{Q}$ to be determined by one quasi-particle excitation, we obtain the single-mode approximation

$$S(\mathbf{Q}, i\omega_n) = \frac{C_{\mathbf{Q}}}{\left(w_n + \Gamma_{\mathbf{Q}}\right)^2 + \varepsilon_{\mathbf{Q}}^2}. \tag{42}$$

Here $\varepsilon_{\mathbf{Q}}$ and $\Gamma_{\mathbf{Q}}$ are the excitation energy and inverse lifetime, respectively, of the quasi-particles, and $C_{\mathbf{Q}}$ is related to the static structure factor of the system. This form of the structure factor leads to an exponential decay of correlations along the world lines according to $S(\mathbf{Q}, \tau) \propto \exp(-\varepsilon_{\mathbf{Q}} |\tau|)$.

In order to understand the physical implications of the single-mode approximation we consider the superfluid phase, where analytical results are available. Eq. (42) is consistent with the two standard sum rules, i.e., the fluctuation-dissipation theorem and the f-sum rule[65], provided that

$$\varepsilon_Q = \frac{Q^2}{2mS(Q)}, \tag{43a}$$

$$C_Q = 2\varepsilon_Q S(Q), \tag{43b}$$

where $S(Q)$ is the static structure factor and all quantities depend only on the magnitude of the wave vector $\mathbf{Q}$ since the superfluid is isotropic. The excitation spectrum ε_Q in Eq. (43a) is the Bijl-Feynman approximation, which, according to the above derivation, is a direct consequence of assuming one quasi-particle to satisfy the standard sum rules. However, it is well known that the Bijl-Feynman approximation significantly overestimates the energy of the excitations in the superfluid, and one excitation therefore does *not* exhaust the sum rules. Nonetheless, we can still assume the single-mode approximation to give a valid description of the dynamic structure factor for small frequencies, and use the form Eq. (42) to fit the numerical data, as illustrated in Fig. 3. The inset shows the corresponding excitation spectrum, the Bijl-Feynman spectrum computed from the static structure factor, and the theoretical Bogoliubov result

$$\varepsilon_Q^B = \frac{\hbar^2}{2m} \sqrt{Q^4 + \frac{4m\rho}{\hbar^2} Q^2 V(Q)}. \tag{44}$$

The agreement is very good for small Q but the Bijl-Feynman approximation seriously overestimates the roton energy. We have not performed an extensive analysis of the systematic errors in our method and the results should therefore be considered as numerical estimates rather than the final result on the excitation spectra in 2D Bose systems.

B. Isobaric Monte Carlo

A disadvantage of performing a simulation of a compressible system at constant density is that a first order transition will not be sharp. Rather, we will observe the coexistence of the two phases at the transition, complicating the interpretation of the data. As was shown in Sec. II, vortices in an applied magnetic field correspond to bosons at fixed chemical potential, and a simulation using the grand canonical ensemble would solve the problem with coexistence. It is, however, technically difficult to vary the number of world lines in the system. Furthermore, by varying the number of world lines, we can only change the density in discrete steps, which is especially problematic for small systems.

Since it is the density rather than the total number of particles which is important, we can instead choose to simulate the Bose system at constant applied pressure. The relevant thermodynamic potential is then the Gibbs free energy, which is defined according to

$$\mathcal{Z}(T, P, N) \equiv \mathrm{e}^{-G(T,P,N)/T} = \int dA \, \mathcal{Z}(T, A, N) \, \mathrm{e}^{-PA/T}, \tag{45}$$

in direct analogy to Eq. (3). The three thermodynamic potentials $F(T, A, N)$, $\Omega(T, A, \mu)$, and $G(T, P, N)$ all offer perfectly valid descriptions of the 2D Bose system, and the choice is therefore a matter of convenience. Since $G(T, P, N)$ does not correspond directly to the experimental situation of a superconductor in an applied magnetic field, we have to make sure that the jump in density is independent on whether we use $G(T, P, N)$ or $\Omega(T, A, \mu)$. We therefore rewrite the free energy according to $F(T, A, N) = Af(T, \rho)$, where $\rho = N/A$. The pressure and the chemical potential are then fixed by the conditions

$$P = \rho \frac{\partial f}{\partial \rho} - f, \tag{46a}$$

$$\mu = \frac{\partial f}{\partial \rho}. \tag{46b}$$

We now consider two phases with free energy densities $f_1(T, \rho_1)$ and $f_2(T, \rho_2)$. The coexistence condition at fixed μ (Ω continuous) is given by

$$\Delta f \equiv f_1 - f_2 = \mu \Delta \rho, \tag{47}$$

where $\Delta\rho = \rho_1 - \rho_2$. The analogous condition at fixed applied pressure (G continuous) is given by

$$\Delta f = \frac{\Delta\rho}{\rho_1}(P + f_1) = \frac{\Delta\rho}{\rho_2}(P + f_2). \tag{48}$$

Comparison with Eq. (46) shows that in both cases we have

$$\Delta f = \frac{\partial f}{\partial \rho}\Delta\rho, \tag{49}$$

which is nothing but the Maxwell construction. The jump in density will therefore be the same irrespective of whether we carry out the simulation at constant P or constant μ. In the language of vortices, this means that the magnetization jumps observed in the simulation are directly comparable to experiments. It is, however, not possible to deduce the strength of the applied magnetic field from the pressure P, just as it is not possible to compute μ from P. According to Eqs. (46) we have $\rho\mu = P + f$, which requires the knowledge of the free energy of the system.

The implementation of the isobaric quantum Monte Carlo algorithm is similar in spirit to the classical case (see, e. g., Ref. 66). Some details, which are mostly of technical nature, are given in Appendix C.

V. NUMERICAL RESULTS FOR THE 2DBCL

One of the advantages of using the Bose model for studying the vortex system numerically is that the algorithm can be tested against known results for bosons. We begin by studying the transition from a Wigner crystal to a superfluid in the 2D Bose Coulomb Liquid, i.e., with $\lambda = \infty$. Fig. 4 shows the structure factor and the superfluid density, computed according to Eq. (34), as a function of Λ. We have used $\beta = 300$ and $M = 100$. The lattice disappears at $\Lambda_m \approx 0.062$, in perfect agreement with the results by Ceperley and Magro using a different numerical technique for the same system[40]. The transition is very sharp: The two structure factors shown as insets correspond to $\Lambda = 0.06205$ and $\Lambda = 0.06245$, so that the relative change in Λ is less than 1%. Simultaneously, the superfluidity rises from $\rho_e = 0$ to $\rho_e = \rho$, showing that the system is either superfluid or a crystal. Since our method of measuring the superfluid density via ρ_e is not well established, we want to make sure that we obtain the same results when measuring ρ_s using the standard winding number definition. Fig. 5 shows the same transition as Fig. 4 for two smaller systems, where the winding number has been measured directly. The dotted vertical line indicates the position of the transition for the larger systems. The curves for the structure factors cross exactly at this line, showing that the position of the transition does not depend on the size of the system. The curves for the superfluid densities cross very close to this line, making us confident that there is only one transition in the system.

The transition from a Wigner crystal to a superfluid is a quantum phase transition, which is driven by a change in $\hbar$ rather than T_B. Since none of the two phases changes dramatically with temperature, the properties of the transition will also not depend strongly on temperature. This can be understood intuitively in the world line picture: The world lines have to be long enough, but not strictly infinitely long. There exists an elegant way to check whether the temperature used in the simulation is low enough to capture the ground state behavior: The free energy of the systems has to be continuous across the transition, which implies

$$\Delta F = \Delta E_{kin} + \Delta E_{pot} - T_B \Delta S = 0. \tag{50}$$

In particular, for the ground state we have $\Delta E_{kin} = -\Delta E_{pot}$ since $T_B = 0$. Fig. 6 shows the kinetic and potential energies for a system with $N = 81$. The transition from a lattice to a superfluid is indicated by a sharp drop in the kinetic energy, about 7%, due to the fact that the particles become delocalized. This decrease in kinetic energy is compensated by an increase in the potential energy. The almost perfect match between kinetic and potential energies in Fig. 6 also shows that the systematic errors in the simulation due to the discretization of the imaginary time are comparable to the statistical error. Thus, we expect our results to hold for the limit $\tau \to 0$, corresponding to continuous lines, and for $\beta \to \infty$, corresponding to zero Bose temperature.

In Fig. 7 we show the energy of the 2DBCL as a function of the de Boer parameter Λ. The transition corresponds to a small change in slope of this curve. The change is more clearly seen in the inset, where we have subtracted the slope of the crystalline phase. Strictly speaking, since we are simulating at a finite temperature, there is a small downward jump in energy in addition to the change of slope. The statistical errors are too large to allow for a reliable estimate of this jump, however.

VI. NUMERICAL RESULTS ON VORTEX LATTICE MELTING

The above results on the transition in the 2DBCL can be directly translated into results for vortex lattice melting. Thus, Fig. 4 shows a first-order melting transition from a lattice into an entangled vortex liquid. As long as we use the approximation $\lambda = \infty$, the entire melting line is given by the value of Λ_m, and we find

$$B_m(T) = \frac{\Phi_0}{\lambda^2}\frac{4\Lambda_m^2}{\sqrt{3}}\frac{\varepsilon_l \varepsilon_0 \lambda^2}{T^2}. \tag{51}$$

This result is not applicable to the low field regime with $a_0 > \lambda$, since the value of Λ_m does depend on the range of the interaction in this regime. For superconductors

that are not too anisotropic, the Lindemann criterion produces the melting line[19],

$$B_m(T) = \frac{\Phi_0}{\lambda^2} 4\pi c_L^2 \frac{\varepsilon^2 \varepsilon_0^2 \lambda^2}{T^2}, \tag{52}$$

which is identical to Eq. (51) with $\varepsilon_l = \varepsilon^2 \varepsilon_0 \ln(a_0/2\sqrt{\pi}\xi)$ and $\Lambda_m \propto c_L^2$. We therefore expect the Bose model to give a good description of vortex lattice melting in YBCO, where the anisotropy, $\varepsilon \approx 1/7$, is moderate. For more anisotropic superconductors, such as BSCCO, the electromagnetic coupling between pancake vortices becomes important, an effect which is not accounted for by the Bose model[47,19]. It is important to remember that the shape of the melting line is mainly determined by the temperature dependence of the characteristic line energy ε_0 rather than by details of the simulation. We will therefore focus on the properties of the melting transition itself, rather than on the shape of the melting line, in this work.

The structure factor shown in Fig. 4 is related to the structure factor measured in small-angle neutron scattering (SANS) experiments[67]. The main difference is that our structure factor measures the correlation in the position of the vortex cores, whereas the neutrons are scattered by the magnetic field of the vortices. This limits the resolution of SANS to length scales larger than the magnetic penetration depth λ.

The elastic theory for the Bose model of the vortex lattice, i.e., with the elastic moduli given in Sec. II B, predicts $\langle u^2 \rangle \propto \Lambda$. Using Eq. (24) it is possible to measure the mean-squared fluctuations numerically, and the result is shown in Fig. 8. The dashed line is a fit to the data for small Λ and we find

$$\langle u^2 \rangle \approx 0.9615\, \Lambda a_0^2. \tag{53}$$

As is seen from the fit, elastic theory works well for $\Lambda \lesssim 0.05$. Closer to the melting transition the renormalization of the elastic moduli becomes important, and the linear dependence of the fluctuations on Λ breaks down. Just below the melting transition we find $\langle u^2 \rangle \approx 0.065$, leading to a Lindemann number of

$$c_L \approx 0.25. \tag{54}$$

This result is in agreement with usual estimates for vortex lattice melting[4].

The amount of entanglement is always very small in the lattice: We typically find $N_e/N \approx 0.026$ just below the transition, compared to $N_e/N \approx 0.56$ in the liquid just above the transition. Entanglement therefore increases by a factor 20 at the transition already for a system with $N = 81$, and we have direct melting into an *entangled* vortex liquid. This is in agreement with recent numerical results on other models[25,26], and with flux transformer experiments[68].

In order to further characterize the melting transition we consider the energy, which was defined in Eq. (36). For the case of vortices, where $\mathcal{Z} = \exp(-\mathcal{F}/T)$, we obtain

$$E = \langle \mathcal{F} \rangle - T \left\langle \frac{\partial \mathcal{F}}{\partial T} \right\rangle. \tag{55}$$

The second term in this expression accounts for the internal temperature dependence in the effective free energy and was neglected in early numerical work on vortex lattice melting, which lead to much too small estimates for the latent heat of the transition.

Although it would be possible to measure the quantity in Eq. (55) directly in a simulation, we adopt a simpler approach here[16]. By direct inspection of the free energy (4) we see that we can make use of the scaling form

$$\mathcal{F}(\{R_i(\tau)\}, T) \approx \varepsilon_0(T) a_0\, \tilde{\mathcal{F}}(\{R_i(\tau)\}), \tag{56}$$

where $\tilde{\mathcal{F}}$ is dimensionless and temperature independent. The approximation only neglects the temperature dependence of $\lambda(T)$ in the interaction, and Eq. (56) therefore becomes exact in the limit $\lambda \to \infty$. Combining Eqs. (55) and (56) we obtain the result

$$E = \langle \mathcal{F} \rangle \left(1 - \frac{T}{\varepsilon_0} \frac{d\varepsilon_0}{dT} \right) = \langle \mathcal{F} \rangle \frac{1+t^2}{1-t^2}, \tag{57}$$

where we have assumed $\varepsilon_0(T) = \varepsilon_0(0)(1-t^2)$ for the last equation. In the simulations, we always measure the quantity $\langle \mathcal{F} \rangle$ and express all results in terms of

$$f \equiv \frac{\langle \mathcal{F} - \mathcal{F}_0 \rangle}{N L_z \varepsilon_0(T)}, \tag{58}$$

where $\mathcal{F}_0$ is the GL free energy for a perfect lattice of lines. Thus, f measures the additional GL free energy, due to thermal fluctuations, per vortex and length in units of $\varepsilon_0(T)$. The real energy of the system can then be easily computed using Eq. (57). In Fig. 9 we show the GL free energy of the vortex system as a function of Λ. The transition is clearly seen as a discontinuity in f with $\Delta f \approx 0.013$. Using Eq. (57), we compute the entropy per vortex and layer and obtain

$$\Delta S = 0.013\,(1+t^2) \frac{\varepsilon_0(0) d}{T_m}, \tag{59}$$

where d is the layer separation. With parameters for YBCO ($d \approx 12$Å, $\lambda_{ab} \approx 1400$Å, and $T_m \approx T_c \approx 92K$) we obtain $\Delta S \approx 0.35 k_B$, in rough agreement with experimental results[13].

It is interesting to consider how much of the latent heat comes from the Josephson energy in our simulation, i.e., from the first term in Eq. (4). It has been shown numerically that approximately half of the latent heat comes from the Josephson energy in a model for a layered superconductor, a relation which is expected to become exact for a line model[26]. Here we reach the same conclusion in a slightly different way: Comparing Eqs. (38) and (40)

we see that the bosonic kinetic energy is the negative of the Josephson energy. Since it was shown above that the changes in kinetic and potential energies for the quantum system have to cancel exactly, it follows that the change in the Josephson energy equals the change in the in-plane interaction energy.

There exist a number of methods for testing numerically whether a transition is first order. A widely used method is to make a histogram of the data for the energy and look for two peaks, indicating the coexistence of two phases[69]. The method did not work very well in the present case, since the transition is too sharp: Coexistence of phases was only observed for small systems, where it is difficult to resolve the two peaks in the energy distribution. The sharpness of the transition for large system is sufficient evidence that the transition is really first order.

We now turn to the case of finite λ, where the system has a finite compressibility. According to the Clausius-Clapeyron relation,

$$\Delta s = -\frac{\Delta B}{4\pi}\frac{dH_m}{dT}, \tag{60}$$

we now expect a change in the density of the vortex system at the transition. When going from the lattice to the liquid phase we have $dH_m/dT < 0$ and $\Delta s > 0$, leading to $\Delta B > 0$. The vortex system therefore shows anomalous melting, just as ice, with the melted phase being the denser one. In the case of the vortex system, the reason for the anomalous behavior can be understood in an intuitive way: When the lines begin to entangle, the line tension will produce an attractive force between them, leading to an increased density[70]. If we assume $H_m \approx B_m$, which is true as long as $\lambda \gtrsim a_0$, we can rewrite Eq. (60) as

$$\Delta f = 8\pi\Delta\rho\lambda(T)^2. \tag{61}$$

Fig. 10 shows the jump in density for two different values of λ. The interaction between the lines is smaller than for $\lambda = \infty$ and the melting transition is shifted towards lower values of Λ_m. The results are summarized in Table I. There is no dramatic change in the properties of the transition when going from $\lambda = \infty$ to $\lambda \approx a_0$. This shows that the logarithmic vortex interaction is a good approximation for most of the phase diagram. The agreement with the Clausius-Clapeyron relation in Eq. (61) is very good for $\lambda = 1.06a_0$, proving that the approximation $H_m \approx B_m$ is valid and that the transition is really first order. For $\lambda = 0.72a_0$, the right hand side of Eq. (61) is too small, since $|dB/dT| < |dH/dT|$. Using the fact that Δf does not depend strongly on λ/a_0, we can use the value $\Delta f \approx 0.013$ and obtain a very simple expression for the density change of the vortex lattice at the melting transition,

$$\Delta\rho \approx 5.2\times10^{-4}/\lambda(T)^2 \Rightarrow \Delta B = \frac{1.1\times10^6\,[\mathrm{G\AA}^2]}{\lambda(T)^2} \tag{62}$$

This expression is again in good agreement with magnetization measurements on YBCO[12].

VII. PROPERTIES OF THE LINE LIQUID

We now turn to the properties of the vortex liquid. It has been shown above that the vortex lattice melts directly into an entangled vortex liquid, which is equivalent to a bosonic superfluid. One important quantity in the vortex liquid is the correlation length l_z in the direction parallel to the lines. If this correlation length grows very large close to the melting line, an apparent disentangled liquid could be observed in a sample of finite thickness. On the other hand, we want the correlation length to be larger than the layer distance in order to separate melting of a line system from decoupling. A lot of experimental effort has been invested into measuring l_z, mainly using flux transformer techniques. The latest results indicate that there exists a short but finite z-axis correlation length in the vortex liquid[71].

One of the nice features of the Bose model is that the question of the z-axis correlation length in the vortex system is related to the fundamental question of the roton minimum in a Bose system. In Sec. II we have shown that the coordinate z along the vortex lines corresponds to the imaginary time τ for bosons. This relation can be made dimensionally correct by writing

$$\frac{g^2\tau}{\hbar} = \frac{2\varepsilon_0 l_z}{T}. \tag{63}$$

According to Eq. 42 we expect the retarded density correlator to decay exponentially, with the characteristic time $\tau_Q = \hbar/\varepsilon_Q$. Using Eq. (63) we obtain[43]

$$l_z(Q) = \frac{T}{2\varepsilon_0}\frac{g^2}{\varepsilon_Q}. \tag{64}$$

The largest correlation length is found for the Q that minimizes ε_Q, i.e., for the roton minimum. Since the roton minimum is located at $Q \approx 2\pi/a_0$, this length is related to the single line correlation length.

Fig. 11 shows the excitation spectra for compressible and incompressible 2D Bose systems. At small Q, the compressible system has a phonon branch, whereas the excitations in the incompressible systems are plasmons. The roton minimum, however, does not change with the range of interaction. Since it is the roton minimum which determines the critical velocity of the superfluid, this supports our claim that the 2DBCL does not differ qualitatively from other 2D Bose liquids with regard to superfluidity. The roton minimum collapses when the system solidifies, indicating 1) the appearance of a periodic lattice and 2) the disappearance of superfluidity. Note that the roton energy is large compared to the Bose temperature used in the simulation, $T_B \approx 0.003\,g^2$ compared to $\varepsilon_{roton} \approx 0.026\,g^2$. This explains why we observe the ground state behavior in the simulation.

Recalculating the roton minimum in terms of Eq. (63) we find

$$l_z\left(\frac{4\pi}{a_0\sqrt{3}}\right) \approx \frac{1}{0.026}\frac{T_m}{2\varepsilon_0} \approx 1.7\sqrt{\frac{\varepsilon_l}{\varepsilon_0}}a_0 \approx 1.7\,\varepsilon a_0. \quad (65)$$

This result is in good agreement with our expectations from elastic theory and scaling theory: The relevant length scale in the lattice is a_0, which should be rescaled by anisotropy. The length l_z is much larger than the layer spacing for YBCO, proving that the transition is really due to melting of continuous lines. As soon as the lattice is formed, l_z becomes infinite and entanglement disappears.

VIII. CONCLUSIONS

We have used the mapping to 2D bosons for studying the vortex system in a high-T_c superconductor numerically. An advantage of this approach is that it allows us to perform the simulation without introducing an artificial lattice, which would cut off small scale fluctuations and introduce spurious pinning effects. Furthermore, by comparing the numerical results to known properties of the corresponding Bose system, we are able to control the systematic errors inherent in any numerical simulation.

We find a first-order vortex lattice melting transition into an entangled vortex liquid. The results for the latent heat and the magnetization jump agree well with experiments for moderately anisotropic superconductors such as YBCO. We do not expect such good agreement for strongly anisotropic materials, since the Bose model describes vortices in terms of elastic lines, rather than pancake vortices, and ignores the electromagnetic coupling between the layers.

In the language of bosons, we have found a sharp transition from a Wigner crystal to a superfluid even for the case of a logarithmic interaction (the 2DBCL). Since the latter system does not have a Bose-Einstein condensate even in the ground state, this shows that the relation between superfluidity and Bose-Einstein condensation is rather subtle. It is amusing to note that the main result in this work can be predicted using two simple physical ideas: 1) the Landau quasi-particle picture and 2) the Bijl-Feynman form for the excitation spectrum in a Bose system.

The emphasis of this work has been on the generic phase diagram for a system of interacting elastic lines. In this picture, the transition described above can be understood in terms of a competition between "energy" and "entropy": The ordered lattice always has the lowest "energy", but there are many more entangled states. The entanglement also offers a natural explanation for the anomalous melting characteristic of vortex lattice. In order for this scenario to work, however, the lines have to be long enough. Thus, one of the main results of this work is to elucidate the importance of the third dimension for vortex lattice melting.

ACKNOWLEDGMENTS

The authors are pleased to acknowledge fruitful discussions with M. Dodgson, M. Feigel'man, E. M. Forgan, V. Geshkenbein, L. Ioffe, A. Koshelev, A. van Otterlo, H. Tsunetsugu, and V. Vinokur. The simulations were carried out using the workstation cluster at the Institute for Theoretical Physics, ETH, and on various computers of the Centro Svizzero di Calcolo Scientifico. Support from the Swiss National Science Foundation is gratefully acknowledged. Work at ANL was funded in part by the NSF-Office of Science and Technology Centers under contract No. DMR91-20000.

APPENDIX A: COMPUTING THE FOURIER SUM FOR THE INTERACTION

We consider a rhombically shaped system with side L and the smaller angle θ. In the simulation we have used $\theta = 60°$, but nothing is lost by solving the more general problem here. Since we want to be able to choose the range of the interaction λ large compared to the size of the system, it is important to account for the periodic boundary conditions in the interaction. In the special case of the vortex interaction this is most easily achieved by solving the London equation using the correct periodic boundary conditions. We introduce a basis $\mathbf{e}_1, \mathbf{e}_2$ with $\mathbf{e}_1 \cdot \mathbf{e}_2 = \cos\theta$. The system is then spanned by the vectors $\mathbf{a}_i = L\mathbf{e}_i$, and the corresponding reciprocal lattice vectors are

$$\mathbf{b}_i = \frac{2\pi}{L\sin^2\theta}\left(\mathbf{e}_i - \mathbf{e}_j\cos\theta\right) \quad (A1)$$

for $(i,j) = (1,2), (2,1)$. The solution to the London equation

$$(1-\lambda^2\Delta)G(\mathbf{R},\lambda) = \lambda^2\delta(\mathbf{R}) \quad (A2)$$

is then given by

$$G(\mathbf{R},\lambda) = \frac{2\pi\lambda^2}{L^2\sin\theta}\sum_{\mathbf{G}}\frac{\mathrm{e}^{i\mathbf{G}\cdot\mathbf{R}}}{1+\lambda^2G^2}, \quad (A3)$$

where the sum is over all reciprocal lattice vectors $\mathbf{G} = n_1\mathbf{b}_1 + n_2\mathbf{b}_2$. This solution is proportional to the magnetic field from one vortex line and in the case of $L \gg \lambda$, the function $G(\mathbf{R},\lambda)$ reduces to $\mathrm{K}_0(R/\lambda)$. Since there is no such simplification for general L, we will have to evaluate the Fourier sum in Eq. (A3) numerically. It is, however, very time consuming to sum over n_1 and n_2 directly, and we have therefore decided to evaluate one of the sums analytically. This can be done with some effort using contour integration, and the resulting expression is

$$G(\mathbf{R},\lambda) = \frac{\sin\theta}{2(1+\cos\theta)}\sum_N \cos(Nt_1)C_N(\lambda,t_2), \quad (A4)$$

with $t_{1,2} = \pi(R_1 \pm R_2)/L$ and

$$C_N(\lambda, t_2) = \begin{cases} \dfrac{\cosh[(\pi/2 - |t_2|)a_N(\lambda)]}{a_N(\lambda)\sinh[\pi a_N(\lambda)/2]}, & N \quad \text{even}, \\ \dfrac{\sinh[(\pi/2 - |t_2|)a_N(\lambda)]}{a_N(\lambda)\cosh[\pi a_N(\lambda)/2]}, & N \quad \text{odd}, \end{cases} \tag{A5}$$

where

$$a_N(\lambda)^2 = \frac{L^2}{2\pi^2\lambda^2}\frac{\sin^2\theta}{1+\cos\theta} + \frac{1-\cos\theta}{1+\cos\theta}N^2. \tag{A6}$$

Eq. (A4) replaces an algebraically converging two-dimensional sum with an exponentially converging one-dimensional one, making the numerical evaluation trivial.

APPENDIX B: SAMPLING PERMUTATIONS

In order to capture the effects of Bose statistics, we have to allow the world lines to switch their endpoints. This can only be done by cutting out sufficiently long segments of a number of lines and trying different ways of connecting the loose ends. Updating the lines therefore becomes a two-step process: First we decide on how to connect the lower ends of the cut with the upper ones and then the new line segments are built up using the bisection method proposed by Ceperley[63].

The problem of connecting the upper and lower ends of a cut of N world lines is difficult for the simple reason that there exist $N!$ ways of doing it. One way around the problem would be to choose only a small number of neighboring lines for the Monte Carlo updates, thus keeping N small. On the other hand, we know that superfluidity is due to large scale particle exchanges; the number of particles participating in a Monte Carlo update has to be large enough to change the winding number of the system. Different approaches have been suggested for solving this problem and some of them can be found in Ref. 63.

The method we use for connecting the ends of the cut is a random walk in the space of permutations. The statistical weight of interconnecting lines is only determined by the kinetic part of the action and we introduce the weight

$$w_{ij} = \exp\left\{-\frac{[\mathbf{R}_j(\tau+\Delta) - \mathbf{R}_i(\tau)]^2}{2\Lambda^2\Delta}\right\} \tag{B1}$$

for connecting the lower end of line i with the upper end of line j over a distance Δ in the imaginary time direction. The total weight of a permutation σ of N lines is then given by

$$W(\sigma) = \prod_{i=1}^{N} w_{i\sigma(i)}. \tag{B2}$$

The probability of the same permutation is the weight normalized by the sum of the weights of all possible permutations, and this normalization factor is practically impossible to compute if N is large. The random walk algorithm selects a permutation in the following way: We first select how to connect the first line with a probability proportional to the weights. Thus, the probability of connecting the lower end of the first line with the upper end of line j is

$$p_{1j} = \frac{w_{1j}}{\sum_{k=1}^{N} w_{1k}}. \tag{B3}$$

After this we select how to connect the second line to any of the remaining $N-1$ lines, again with the probability proportional to the weight. The procedure is repeated until all lines have been connected. The acceptance probability for this permutation is then given by

$$A(\sigma) = \prod_{k=1}^{N} \frac{\sum_{l=k}^{N} w_{k\sigma(l)}}{\sum_{l=k}^{N} w_{kl}}. \tag{B4}$$

If the permutation is not accepted, the random walk is started again. The algorithm is exact as long as the identity permutation is the cheapest permutation, i.e., as long as $A(\sigma) \leq 1$ for all possible permutations, something which is almost always true even in the superfluid phase. It is still not possible to sample the permutations of arbitrarily large systems since the acceptance rate decreases with N and it becomes necessary to try very many random walks before an acceptable permutation is found. However, since the weights w_{ij} can be computed once and stored in a table, each random walk is very fast. Using this algorithm we were able to sample the permutations of $N \leq 49$ particle almost exactly. For larger systems, we typically restricted ourselves to $N \approx 25$ neighboring lines.

APPENDIX C: ISOBARIC MONTE CARLO ALGORITHM

In order to implement the isobaric Monte Carlo method, we first rewrite the discretized action (22) using the system size L as a length scale,

$$S[\{\mathbf{x}_i\}, L] = L^2 \sum_{i,m} \frac{(\mathbf{x}_{i,m+1} - \mathbf{x}_{i,m})^2}{2\Lambda^2\tau} - MN\ln(L^2) + \sum_{i<j,m} \tau \mathrm{K}_0\left(\frac{L x_{ij,m}}{\lambda}\right) + \beta P L^2. \tag{C1}$$

Here we have added a term corresponding to the external pressure (cf. Eq. (45)) and a logarithmic term coming from the change of variable, $\mathbf{R} = L\mathbf{x}$, in the integral

$$\int \prod_{m=1}^{M}\prod_{i=i}^{N} d^2R_{i,m} = \mathrm{e}^{MN\ln(L^2)} \int \prod_{m=1}^{M}\prod_{i=i}^{N} d^2x_{i,m}. \tag{C2}$$

Using Eq. (C1) we can compute the change in all thermodynamic quantities as a function of the area of the system. The only problem is with the interaction term, which does not scale in a simple way with the area. In the present simulation, the interaction is stored in a lookup table and it would be too time consuming to reinitialize these tables every time the volume changes. We are helped by the fact that the volume changes are small, allowing us to use a Taylor expansion,

$$U\left[L^2(1+\varepsilon)\right] \approx U(L^2) + L^2\frac{dU}{d(L^2)}\varepsilon + \frac{1}{2}L^4\frac{d^2U}{d(L^2)^2}\varepsilon^2, \tag{C3}$$

where

$$U(L^2) = \sum_{i<j,m} \tau \mathrm{K}_0\left(Lx_{ij,m}/\lambda\right). \tag{C4}$$

The interaction and its two derivatives with respect to the area are evaluated for fixed L during the simulation. As long as the changes in L are small, we can use the Taylor expansion for evaluating the change in Eq. (C1).

Rather than sampling the fluctuations in L, we used Eq. (C1) to optimize the action with respect to L after the line configuration has been updated once. This gives the correct expectation value for the density and the other thermodynamic quantities.

[1] A. A. Abrikosov, Sov. Phys. JETP **5**, 1174 (1957).
[2] L. D. Landau, Sov. Phys. JETP **7**, 627 (1937).
[3] E. Brézin, D. R. Nelson, and A. Thiaville, Phys. Rev. B **31**, 7124 (1985).
[4] G. Blatter *et al.*, Rev. Mod. Phys. **66**, 1125 (1994).
[5] M. V. Feigelman, V. B. Geshkenbein, L. B. Ioffe, and A. I. Larkin, Phys. Rev. B **48**, 16641 (1993).
[6] T. Chen and S. Teitel, Phys. Rev. Lett. **76**, 714 (1996).
[7] G. Eilenberger, Phys. Rev. **164**, 628 (1967).
[8] R. Labusch, Phys. Status Solidi **32**, 439 (1969).
[9] H. Safar *et al.*, Phys. Rev. Lett. **69**, 824 (1992).
[10] M. Charalambous, J. Chaussy, and P. Lejay, Phys. Rev. B **45**, 5091 (1992).
[11] E. Zeldov *et al.*, Nature **375**, 373 (1995).
[12] U. Welp *et al.*, Phys. Rev. Lett. **76**, 4809 (1996).
[13] A. Schilling *et al.*, Nature **382**, 791 (1996).
[14] M. Roulin, A. Junod, and E. Walker, Science **273**, 1210 (1996).
[15] J. Hu and A. H. MacDonald, Phys. Rev. B **56**, 2788 (1997).
[16] M. J. W. Dodgson, V. B. Geshkenbein, H. Nordborg, and G. Blatter, Phys. Rev. Lett. **80**, 837 (1998).
[17] S. Sengupta *et al.*, Phys. Rev. Lett. **67**, 3444 (1991).
[18] A. Houghton, R. A. Pelcovits, and A. Sudbø, Phys. Rev. B **40**, 6763 (1989).
[19] G. Blatter, V. B. Geshkenbein, A. I. Larkin, and H. Nordborg, Phys. Rev. B **54**, 72 (1996).
[20] A. M. Schönenberger, V. B. Geshkenbein, and G. Blatter, Phys. Rev. Lett. **75**, 1380 (1995).
[21] Y.-H. Li and S. Teitel, Phys. Rev. Lett. **66**, 3301 (1991).
[22] R. E. Hetzel, A. Sudbø, and D. A. Huse, Phys. Rev. Lett. **69**, 518 (1992).
[23] Y.-H. Li and S. Teitel, Phys. Rev. B **47**, 359 (1993).
[24] T. Chen and S. Teitel, Phys. Rev. B **55**, 11766 (1996).
[25] X. Hu, S. Miyashita, and M. Tachiki, Phys. Rev. Lett. **79**, 3498 (1997).
[26] A. E. Koshelev, Phys. Rev. B **56**, 11201 (1997).
[27] A. K. Nguyen and Sudbø, Phys. Rev. B **57**, 3123 (1998).
[28] A. K. Nguyen and A. Sudbø, Phys. Rev. B **58**, ???? (1998).
[29] T. Chen and S. Teitel, Phys. Rev. Lett. **74**, 2792 (1995).
[30] G. Carneiro, Phys. Rev. Lett. **75**, 521 (1995).
[31] A. K. Nguyen, A. Sudbø, and R. E. Hetzel, Phys. Rev. Lett. **77**, 1592 (1996).
[32] T. J. Hagenaars, E. H. Brandt, R. E. H. W. H. M. Leghissa, and G. Saemann-Ischenko, Phys. Rev. B **55**, 11706 (1997).
[33] R. Šášik and D. Stroud, Phys. Rev. Lett. **75**, 2582 (1995).
[34] D. R. Nelson, Phys. Rev. Lett. **60**, 1973 (1988).
[35] D. R. Nelson and V. M. Vinokur, Phys. Rev. B **48**, 13060 (1993).
[36] N. Hatano and D. R. Nelson, Phys. Rev. Lett. **77**, 570 (1996).
[37] U. C. Täuber and D. R. Nelson, Physics Reports **289**, 157 (1997).
[38] C. E. Campbell, in *Progress in Liquid Physics*, edited by C. A. Croxton (Wiley, New York, 1978), Chap. 6, p. 213.
[39] L. Pitaevskii and S. Stringari, J. Low Temp. Phys. **85**, 377 (1991).
[40] W. R. Magro and D. M. Ceperley, Phys. Rev. Lett. **73**, 826 (1994).
[41] H. Nordborg and G. Blatter, Phys. Rev. Lett. **79**, 1925 (1997).
[42] R. P. Feynman, *Statistical Mechanics* (Addison-Wesley, Redwood City, 1972).
[43] D. R. Nelson and H. S. Seung, Phys. Rev. B **39**, 9153 (1989).
[44] S. Ryu and D. Stroud, Phys. Rev. Lett. **78**, 4629 (1997).
[45] G. Blatter, V. B. Geshkenbein, and A. I. Larkin, Phys. Rev. Lett. **68**, 875 (1992).
[46] A. Sudbø and E. H. Brandt, Phys. Rev. Lett. **66**, 1781 (1991).
[47] L. I. Glazman and A. E. Koshelev, Phys. Rev. B **43**, 2835 (1991).
[48] G. Blatter and V. B. Geshkenbein, Phys. Rev. Lett. **77**, 4958 (1996).
[49] J. M. Caillol, D. Levesque, J. J. Weis, and J. P. Hansen, J. Stat. Phys. **28**, 325 (1982).
[50] S. W. de Leeuw and J. W. Perram, Physica A **113**, 546 (1982).
[51] P. Choquard and J. Clerouin, Phys. Rev. Lett. **26**, 2086 (1983).
[52] J. M. Kosterlitz and D. J. Thouless, J. Phys. C **6**, 1181 (1973).
[53] A. F. Andreev and I. M. Lifshitz, Sov. Phys. JETP **29**, 1107 (1969).
[54] M. W. Meisel, Physica B **178**, 121 (1992).
[55] A. van Otterlo and K.-H. Wagenblast, Phys. Rev. Lett. **72**, 3598 (1994).

[56] E. Frey, D. R. Nelson, and D. S. Fisher, Phys. Rev. B **49**, 9723 (1994).
[57] N. D. Mermin and H. Wagner, Phys. Rev. Lett. **17**, 1133 (1966).
[58] W. R. Magro and D. M. Ceperley, Phys. Rev. B **48**, 411 (1993).
[59] S. Zhang, N. Kawashima, J. Carlson, and J. E. Gubernatis, Phys. Rev. Lett. **74**, 1500 (1995).
[60] E. L. Pollock and D. M. Ceperley, Phys. Rev. B **30**, 2555 (1984).
[61] E. L. Pollock and D. M. Ceperley, Phys. Rev. B **36**, 8343 (1987).
[62] D. M. Ceperley and E. L. Pollock, Phys. Rev. B **39**, 2084 (89).
[63] D. M. Ceperley, Rev. Mod. Phys. **67**, 279 (1995).
[64] M. Jarrell and J. E. Gubernatis, Physics Reports **269**, 133 (1996).
[65] A. L. Fetter and J. D. Walecka, *Quantum Theory of Many-Particle Systems* (McGraw-Hill, New York, 1971).
[66] M. P. Allen and D. J. Tildesley, *Computer Simulation of Liquids* (Clarendon Press, Oxford, 1987).
[67] R. Cubitt *et al.*, Nature **365**, 407 (1993).
[68] D. López, E. F. Righi, G. Nieva, and F. de la Cruz, Phys. Rev. Lett. **76**, 4034 (1996).
[69] J. Lee and J. M. Kosterlitz, Phys. Rev. Lett. **65**, 137 (1990).
[70] D. R. Nelson, Nature **375**, 356 (1995).
[71] E. F. Righi *et al.*, Phys. Rev. B **55**, 14156 (1997).

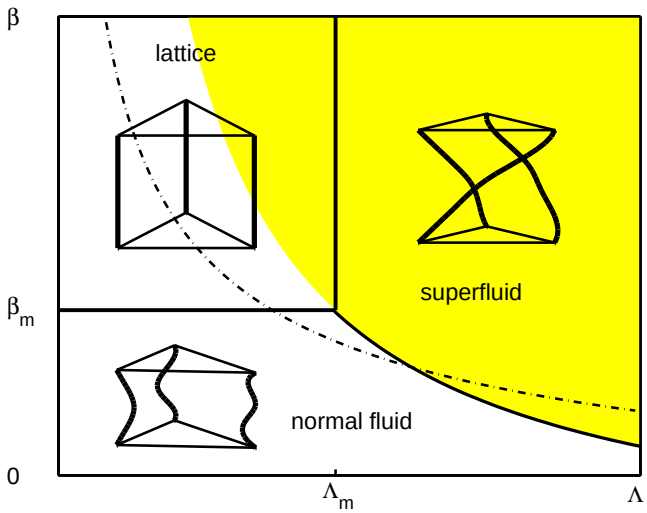

FIG. 1. Schematic phase diagram of the 2DBCL in the parameters Λ and β. The solid lines indicate real phase transitions and quantum effects are important in the shaded region. For vortices in high-T_c superconductors we have $\Lambda^2 = T^2/2\varepsilon_l\varepsilon_0 a_0^2$ and $\beta = 2\varepsilon_0 L_z/T$. The dashed line is obtained by keeping B (a_0) fixed and varying T. This line passes through all three phases for thin samples and is shifted to larger β as L_z is increased.

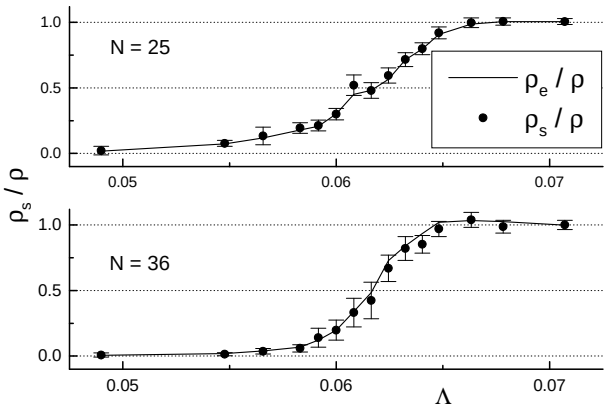

FIG. 2. The superfluid density of the 2DBCL measured using the winding number (dots) and the entanglement density (solid line) as explained in the text. We have used the parameters $\beta = 300$, $M = 100$, and $N = 25, 36$. Both curves are fitted using the value $\alpha(\Lambda, \beta) = 4.04$, which was established by requiring the last point ($\Lambda \approx 0.071$) to have $\rho_e = \rho$.

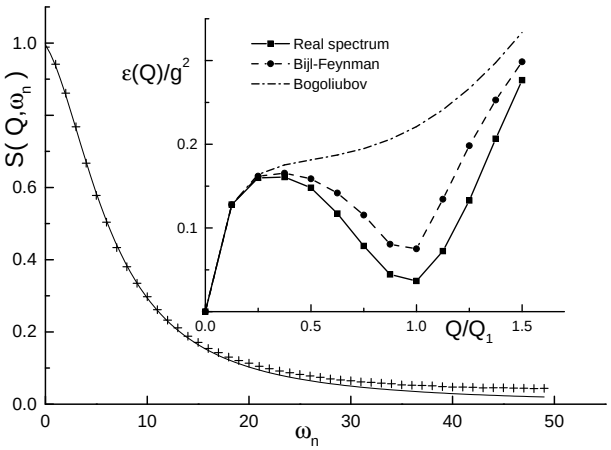

FIG. 3. Fit of the single mode structure factor $S(Q, i\omega_n)$ to measured data for a compressible system with $N = 64$, $M = 100$, and $\beta = 300$ at $Q/Q_1 = 0.5$. The fit is very good for low frequencies and fails for higher ones as expected. The inset shows the excitation spectrum obtained from our method compared to the Bijl-Feynman and Bogolioubov spectra.

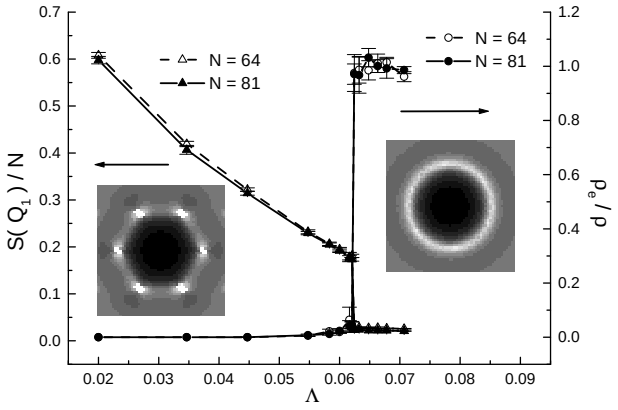

FIG. 4. Structure factor and superfluid density at the transition from a Wigner crystal to a superfluid for the 2DBCL. We have used parameters $\beta = 300$, $M = 100$, and $N = 64, 81$, and have measured the superfluid density using ρ_e as described in the text. The peaks in the structure factor disappear in a sharp transition at $\Lambda \approx 0.062$. Simultaneously, the superfluid density rises from $\rho_e \approx 0$ to $\rho_e \approx \rho$. The transition is very sharp, with a relative error $\Delta\Lambda/\Lambda < 1\%$. In the language of vortices, the data shows a first-order vortex lattice melting transition into an entangled vortex liquid.

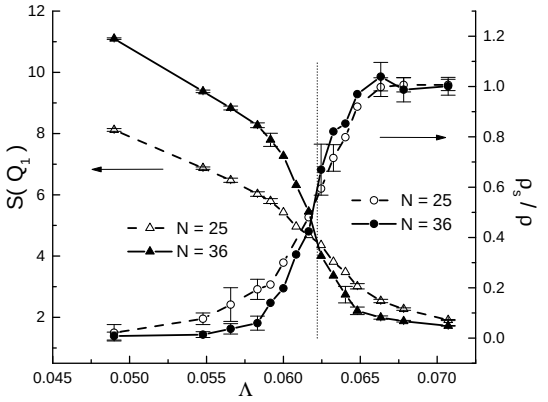

FIG. 5. The same transition as in Fig. 4 for smaller systems with $N = 25, 36$. The superfluid density is measured directly through the winding number. The vertical dotted line shows the position of the transition for the larger systems in Fig. 4. The curves for the structure factor cross at this line, showing that the position of the transition is not shifted with the size of the system. The curves for the superfluid density also cross very close to the vertical line, although the statistical errors are larger. We have removed the error bars from some data points for clarity.

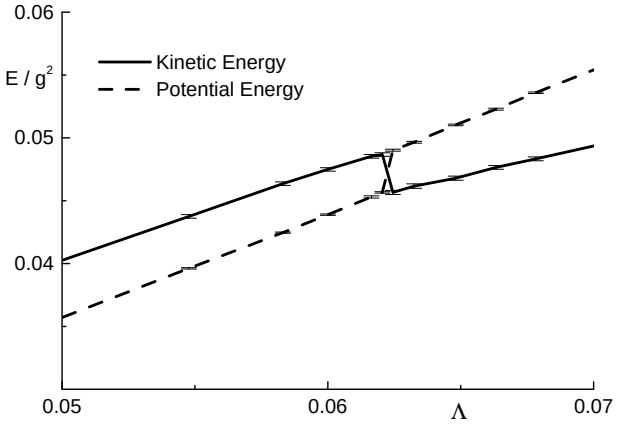

FIG. 6. Potential and kinetic energies at the transition from lattice to superfluid for the 2DBCL with $N = 81$ and $\beta = 300$. The mismatch in energy is less than 10% of the total jump, which is comparable to the statistical error. The relative change in kinetic energy at the transition is 7%. The potential energy has been shifted an arbitrary amount for clarity.

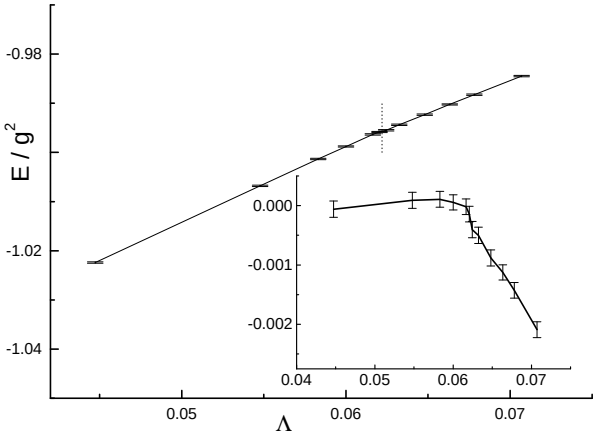

FIG. 7. Energy of the 2DBCL as a function of Λ for a system with $N = 81$, $M = 100$, and $\beta = 300$. The transition, indicated by the vertical dotted line, corresponds to a change in slope. This can be seen more clearly in the inset, where we plot $E - c\Lambda$ and have chosen c to match the slope below the transition.

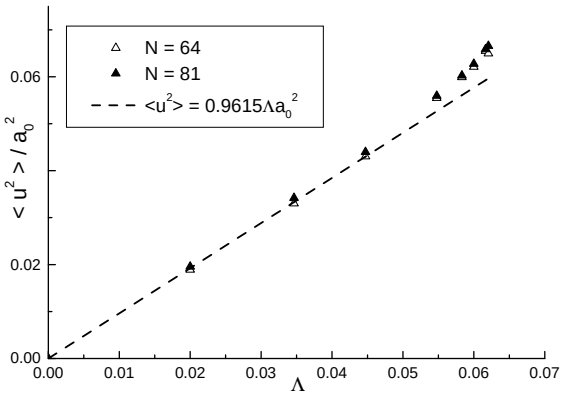

FIG. 8. Mean squared fluctuations of in the vortex system. The data points were obtained from the structure factor in Fig 4. The dashed line is a fit to the data for small Λ and gives $\langle u^2 \rangle \approx 0.9615\,\Lambda a_0^2$. The simple linear behavior breaks down for $\Lambda > 0.05$ due to renormalization of the elastic moduli. The Lindemann number computed from the size of the fluctuations just before melting is $c_L \approx 0.25$.

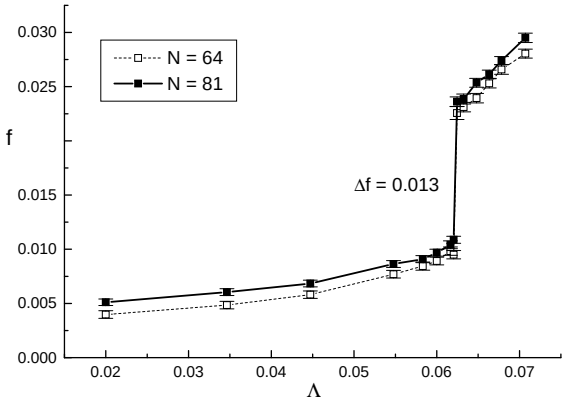

FIG. 9. The GL free energy per particle and length for vortices with $\lambda = \infty$. The energy of a perfect vortex lattice has been subtracted. The melting transition is clearly seen as a discontinuity in the energy, $\Delta f \approx 0.013$. The same systems as in Fig. 4 were used.

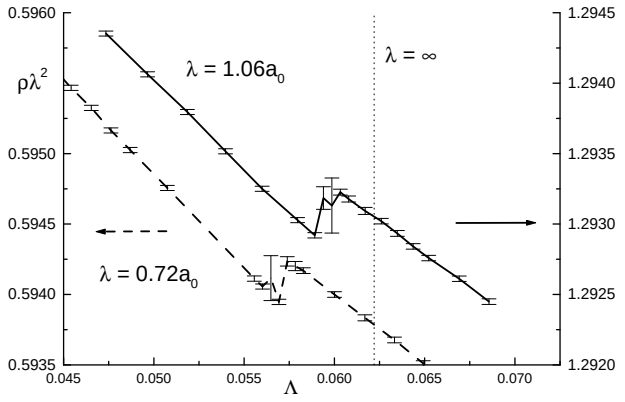

FIG. 10. The change in density for two systems simulated with the isobaric Monte Carlo method. We have used the parameters $\beta = 300$, $M = 100$, and $N = 64$. The vertical dotted line indicates the position of the transition in the 2DBCL. The transition is shifted to smaller values of Λ as a result of the weaker interaction.

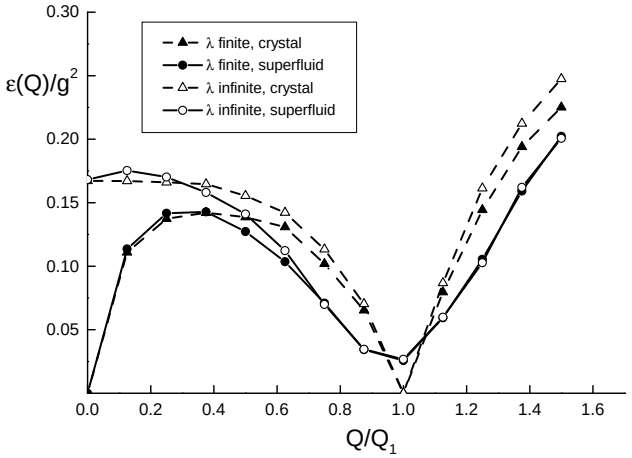

FIG. 11. Comparison of the excitation spectra for compressible and incompressible systems. The parameters are $\beta = 300$, $M = 100$, $N = 64$, and the compressible system has $\lambda \approx 1.06 a_0$. The compressible system has a phonon branch for small Q. As the range of interaction is increased, the phonons turn into plasmons. The roton minimum is independent of the range of interaction, but collapses as the system crystallizes.

TABLE I. Jump in energy and density for three systems with $N = 64$, $\beta = 300$, and $M = 100$ at different pressures. The relative error is less than 5% in the measured quantities

P	λ/a_0	Λ_m	Δf	$8\pi\lambda^2\Delta\rho$
∞	∞	0.0622	0.0127	–
5	1.06	0.0596	0.0113	0.0116
1	0.72	0.0567	0.0091	0.0085